A 3D diffusional-compartmental model of the calcium dynamics in cytosol, sarcoplasmic reticulum and mitochondria of murine skeletal muscle fibers

Lorenzo Marcucci[1]*, Marta Canato[1], Feliciano Protasi[2,3], Ger J. M. Stienen[4], Carlo Reggiani[1]

1 Department of Biomedical Sciences, University of Padova, Padova, Italy, 2 CeSI-Met - Center for Research on Ageing and Translational Medicine, Chieti, Italy, 3 Department of Medicine and Aging Science; University G. d'Annunzio, Chieti, Italy, 4 Department of Physiology, VU University Medical Centre, Amsterdam Cardiovascular Sciences, Amsterdam, the Netherlands

* lorenzo.marcucci@gmail.com

Abstract

Variations of free calcium concentration ($[Ca^{2+}]$) are powerful intracellular signals, controlling contraction as well as metabolism in muscle cells. To fully understand the role of calcium redistribution upon excitation and contraction in skeletal muscle cells, the local $[Ca^{2+}]$ in different compartments needs to be taken into consideration. Fluorescent probes allow the determination of $[Ca^{2+}]$ in the cytosol where myofibrils are embedded, the lumen of the sarcoplasmic reticulum (SR) and the mitochondrial matrix. Previously, models have been developed describing intracellular calcium handling in skeletal and cardiac muscle cells. However, a comprehensive model describing the kinetics of the changes in free calcium concentration in these three compartments is lacking. We designed a new 3D compartmental model of the half sarcomere with radial symmetry, which accounts for diffusion of Ca^{2+} into the three compartments and simulates its dynamics at rest and at various rates of stimulation in mice skeletal muscle fibers. This model satisfactorily reproduces both the amplitude and time course of the variations of $[Ca^{2+}]$ in the three compartments in mouse fast fibers. As an illustration of the applicability of the model, we investigated the effects of Calsequestrin (CSQ) ablation. CSQ is the main Ca^{2+} buffer in the SR, localized in close proximity of its calcium release sites and near to the mitochondria. CSQ knock-out mice muscles still preserve a near-normal contractile behavior, but it is unclear whether this is caused by additional SR calcium buffering or a significant contribution of calcium entry from extracellular space, via stored-operated calcium entry (SOCE). The model enabled quantitative assessment of these two scenarios by comparison to measurements of local calcium in the cytosol, the SR and the mitochondria. In conclusion, the model represents a useful tool to investigate the impact of protein ablation and of pharmacological interventions on intracellular calcium dynamics in mice skeletal muscle.

Introduction

The cytosolic calcium concentration ($[Ca^{2+}]_{cyto}$) plays a crucial role in the regulation of muscle contraction and relaxation [1]. In parallel with its role in regulating muscle activity, calcium also regulates ATP resynthesis in the mitochondria. Therefore, insight into the local variation in the intracellular Ca^{2+}-concentration is key to understand not only the link between excitation and contraction but also its role in maintaining the balance between ATP demand and supply. The calcium-mediated regulation is critically dependent on the calcium release units (CRUs), the specialized intracellular junctions, also named triads, which are formed by the apposition of the terminal cisternae (TC) of the sarcoplasmic reticulum (SR) and the transverse tubuli (TT). The intermyofibrillar mitochondria are located near to the CRUs. Among the most important proteins composing the CRUs there are the dihydropiridine receptor (DHPR), acting as a voltage sensor, the ryanodine receptor (RyR), which is the TC calcium release channel, the SR Ca^{2+} buffer calsequestrin (CSQ), and the junctional proteins triadin and junctin. Mutations of these proteins are known to cause severe disorders and diseases, such as Malignant Hyperthermia (MH), Central Core Disease (CCD), and Vacuolar Myopathy (see for recent reviews [2,3]).

In skeletal and cardiac muscle cells, calcium ions are stored in the TC of the SR which are in close contact with the TT system, which propagates the action potential (AP) during excitation-contraction (EC) coupling. The AP triggers the release of calcium through the interaction between DHPR and RyR, so that calcium can diffuse in the cytosol. The binding of calcium to the Tn-C subunit of troponin induces a shift of the tropomyosin filament on the actin filament uncovering the actin-binding sites for myosin and allowing for the beginning of the acto-myosin cycle and force generation with the associated chemical energy (ATP) utilization. The release of calcium via RyR channels, its binding to cytosolic buffers, and the re-uptake back into SR through the sarcoplasmic endoplasmic reticulum calcium ATPases (SERCA) determines the amplitude and the time course of the cytosolic calcium ($[Ca^{2+}]_{cyto}$) transient. When the RyR channels are closed (low RyR permeability), $[Ca^{2+}]_{cyto}$ drops below the threshold required to activate the actin filaments and the muscle relaxes. Ca^{2+} uptake in the mitochondria plays an important role in modulating the resynthesis of ATP required for force generation and SR Ca^{2+} reuptake via SERCA.

Previously, models have been developed describing intracellular calcium handling in skeletal and cardiac muscle cells [4–10]. Evidence suggests that the local calcium concentrations and the calcium diffusion within the cell need to be taken into consideration [11]. Moreover, insight in the dynamics of $[Ca^{2+}]$ in all the intracellular compartments is a requirement for a full understanding of the calcium cycle triggered by APs [9]. A comprehensive model describing the kinetics of the changes in free calcium concentration in skeletal muscle fibers, and integrating the two above features, is still lacking. Therefore, we designed a 3D compartmental model which takes into account the radial symmetry of the unit cell of striated muscle (the half sarcomere) to simulate calcium dynamics at rest and during trains of stimulation at various rates in mice skeletal muscle fibers. The model includes a cytosolic compartment where myofibrils are located, a sarcoplasmic reticulum compartment to which TC are associated and a mitochondrial compartment. The experimental data for model validation are provided by determination of free calcium concentration in the cytosolic compartment $[Ca^{2+}]_{cyto}$ with ratiometric probes such as Fura 2. The determination of $[Ca^{2+}]$ in the other two most relevant intracellular compartments, the lumen of the sarcoplasmic reticulum (SR) and the mitochondrial matrix, can be achieved by more recently developed genetically targeted FRET-based fluorescent probes [12–15].

To validate our model, we first simulated the variations of free and bound [Ca^{2+}] during contractile activity in the three compartments. As a further test and an illustration of the applicability of the model we investigated the effects of Calsequestrin (CSQ) ablation. In our laboratories, wild type mice and mice carrying null mutations of the genes coding for calsequestrin (CSQ-KO) have been comparatively studied for several years [12,13,16–21]. Surprisingly, CSQ knock-out mice muscles still preserve a near-normal contractile behavior, but it is unclear whether this is caused by calcium storage in additional SR Ca^{2+} buffers or by a significant contribution of Ca^{2+} entry from extracellular space, when the SR is depleted of Ca^{2+}, via stored-operated Ca^{2+} entry (SOCE). The model enabled quantitative assessment of these two scenarios by comparison with measurements of local calcium in the cytosol, the SR and the mitochondria.

Material and methods

Modelling Ca^{2+} movements

Skeletal muscle cells are composed of a parallel arrangement of thin myofibrils of approximately 1 μm in diameter, consisting of 2.5 μm long sarcomeres surrounded by a sarcoplasmic reticular network and mitochondria. The half sarcomere can be considered as the unit cell with cylindrical geometry, from M-line to Z-line, with a radius R = 0.5 μm and a length L = 1.25 μm (values are summarized in S1 Table), with three compartments: 1. the SR in the most outer region, with a TC at the end of the thick filaments, 2. the cytosolic space where myofibrils are located and 3. the mitochondrion, in the cytosolic space near the TC (see Fig 1). The contribution of subsarcolemmal and perinuclear mitochondria to intracellular Ca^{2+} handling is assumed to be negligible in this configuration.

The SR occupies 9% of the total volume (V$_{tot}$) including the TC, which accounts for 3.5% of the total volume V$_{tot}$ [22]. The cytosolic space equals the sum of myofibrillar space (MS, 80% of V$_{tot}$), which contains the myofibrils, and extramyofibrillar space (EF, 6% of V$_{tot}$), closer to SR. The remaining 5% of V$_{tot}$ is occupied by mitochondria [13,23,24].

Ca^{2+} fluxes between the compartments are controlled by Ca^{2+}-pumps or channels, but Ca^{2+} can also diffuse within the SR and cytosolic space with a free diffusion coefficient (D) of 300 μm^{2}s^{-1} [7]. The half-sarcomere is divided into m = 10 longitudinal (1 being adjacent to M-line, see Fig 1) and n = 5 radial (1 being the center of muscle cell) sub-compartments. Myofibrils occupy radial compartments from 1 to 3, the 4th being the EF, and are surrounded by the SR. TC, where Ca^{2+} release takes place, are located in the 7th longitudinal compartment of the 5th radial sub-compartment, at a distance of approximatively 0.8 μm from the M-line. SERCA is located along all the SR compartments. Mitochondrial influx and efflux are based on the local [Ca^{2+}]$_{cyto}$ in the 8th longitudinal and 4th radial sub-compartment, 125 nm away from RyR. The distribution of these elements has been chosen to closely match the observed average position of mitochondria at about 130 nm distance from the TC [11,25]. The results obtained for Ca^{2+} signal in frog skeletal muscle from an 18- and a 100-compartments model have been reported to be close each other [26]. Similarly, we have compared the results for our 50-compartments model, to a finer model with m = 20 and n = 15 (300 compartments). In the finer model, average cytosolic calcium decreases by only 3%, while oscillations in the compartment with the MCU and NCE (125 nm away from the RyR), maximum [Ca^{2+}] increases by 9% (from 870 to 950 nM), while the minimum is almost stable at 240 nM (see S1 Fig). Similar differences are observed also in the free [Ca^{2+}]$_{mito}$, however, the difference in the average values is less than 0.1%. Therefore the 50-compartments model is used in the simulations which also has the advantage that the computation time is suitable on a common personal computer using MatLab.
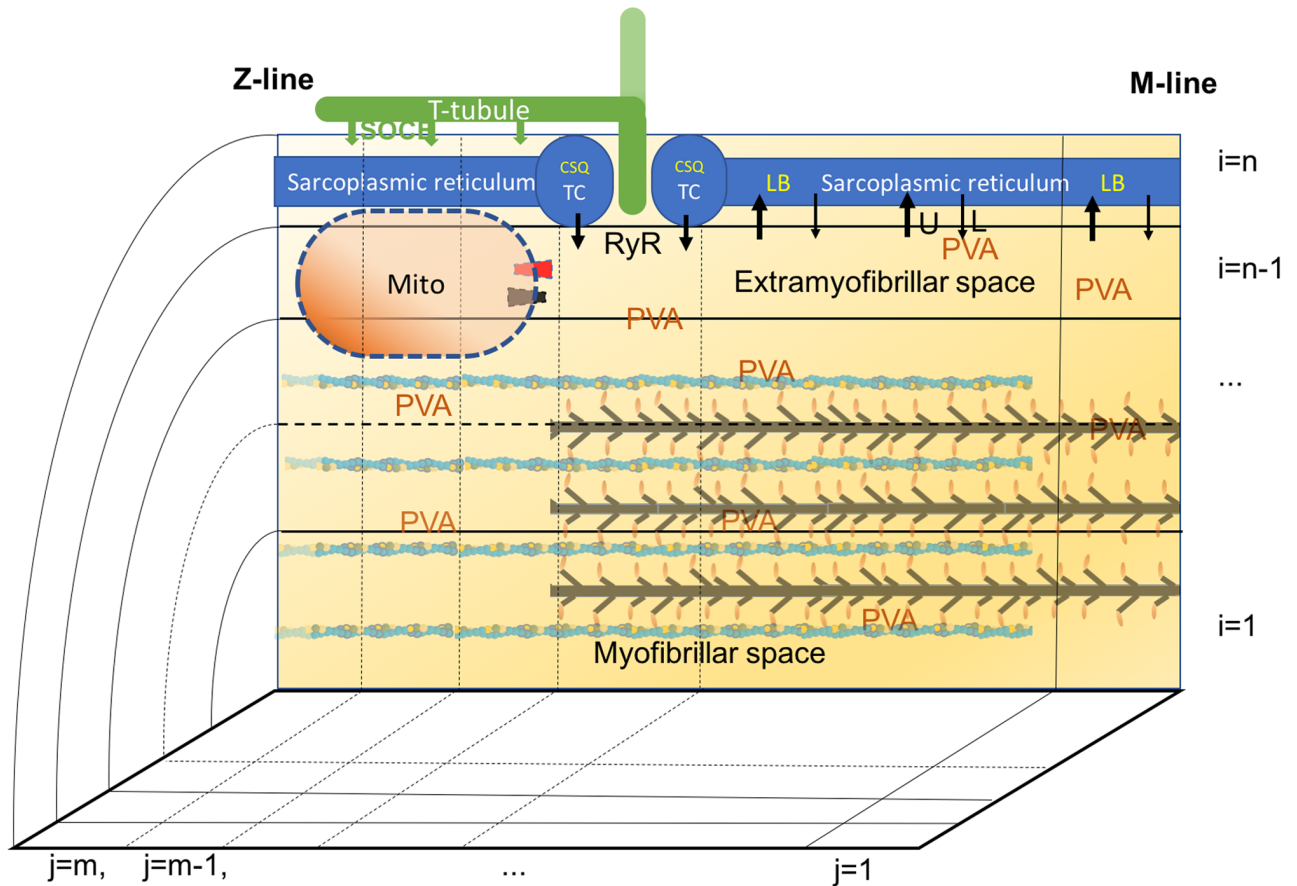
Fig 1. Schematic representation of the 3D compartmental diffusional model of murine skeletal muscle. The unit cell of the skeletal muscle fiber, the half sarcomere, is approximated as a cylinder, so that rotational symmetry allows for analysis in 2D space. This space is occupied by three main compartments: sarcoplasmic reticulum, cytosolic space and mitochondrion. The sarcoplasmic reticulum is divided into m longitudinal sub-compartments and the cytosolic space is divided into m longitudinal and n-1 radial sub-compartments. Diffusion of Ca²⁺ ions is analyzed between sub-compartments. The mitochondrial compartment is close, but external, to extramyofibrillar space (EF). The mitochondrial calcium uniporter (MCU in black) and sodium calcium exchanger (NCE in red) sense the [Ca²⁺] in the sub-compartment 125 nm away from the RyR, toward Z-line. Several buffers are present in distinct sub-compartments: calsequestrin (CSQ) and additional buffers (AB) in sarcoplasmic reticulum, parvalbumin (PVA) in all cytosolic spaces, troponin in the myofibrillar spaces, and a mitochondrial buffer (B) in the mitochondrial matrix. Store operated Ca²⁺ entry (SOCE) is depicted by the vertical arrows from the T-tubular network extended toward the Z-line (green).

https://doi.org/10.1371/journal.pone.0201050.g001

The cylindrical geometry makes the equation for the rate of the local change in $[\text{Ca}^{2+}]$ [27]:

$$\frac{\partial [\text{Ca}^{2+}]}{\partial t} = \frac{1}{r}\frac{\partial}{\partial r}\left[Dr\frac{\partial [\text{Ca}^{2+}]}{\partial r}\right] + \frac{\partial}{\partial x}\left[D\frac{\partial [\text{Ca}^{2+}]}{\partial x}\right] - F([\text{Ca}^{2+}], t) \tag{1}$$

in which x is the longitudinal coordinate and r the radial one, and F is the net binding flux. Using the discretization as proposed previously [4] this equation becomes:

$$\frac{[\text{Ca}^{2+}]_{i,j,t+\Delta t} - [\text{Ca}^{2+}]_{i,j,t}}{\Delta t} = 4Dn/R^2[i([\text{Ca}^{2+}]_{i+1,j} - [\text{Ca}^{2+}]_{i,j}) - (i-1)([\text{Ca}^{2+}]_{i,j} - [\text{Ca}^{2+}]_{i-1,j})]$$

$$ + D\left(\frac{m}{L}\right)^2 [[\text{Ca}^{2+}]_{i,j+1} - 2[\text{Ca}^{2+}]_{i,j} + [\text{Ca}^{2+}]_{i,j-1}] - F([\text{Ca}^{2+}]_{i,j}, t). \tag{2}$$

Ca²⁺ ions can exit from SR to EF through RyR channel present in the TC, whose permeability is regulated by the action potential. Following the analysis and constraints proposed in [4],

we assume that the permeability (P_t) increases and decreases exponentially with time constants $\tau_{on} = 1$ ms and $\tau_{off} = 5$ ms. Then, the rate of Ca2+ release is:

$$\left.\frac{dCa^{2+}}{dt}\right|_{RyR} = P_{max}\left[1 - e^{-\frac{t}{\tau_{on}}}\right]\left[e^{-\frac{t}{\tau_{off}}}\right]\left([Ca^{2+}]_{TC} - [Ca^{2+}]_x\right) \tag{3}$$

where P_{max} is the maximum permeability which includes the release surface of the TC. The rate of release depends on the gradient of $[Ca^{2+}]$ between the TC and the sub-compartment of EF adjacent to TC (subscript x). Actually, the rate of calcium release depends on several factors which have been collected in the parameter "evacuability" [15,28], which includes permeability, release surface and intraluminal buffering. Following the procedure proposed previously [4] we fit the parameter P_{max} to obtain the experimentally observed averaged $[Ca^{2+}]_{cyto}$ in WT mice during the steady phase of the train of stimuli. This approach does not take calcium dependent inactivation into account. A reduction in the Ca2+ release flux from the first AP to the second and subsequent has been considered in previous models [7] to account for calcium dependent inactivation. In this study, we focus on the $[Ca^{2+}]$ in the three compartments during the steady phase, reached toward the end of a stimulation train. Therefore, we decided not to include such a phenomenon. The impact of calcium dependent inactivation, as described previously (27), in the present model is illustrated and discussed in the S1 File.

SERCA activity is modeled by simplified first-order kinetics proposed by [4], as follows:

$$\left.\frac{dCa^{2+}}{dt}\right|_{Up} = \frac{V_{max}[Ca^{2+}]_{EFx}}{[Ca^{2+}]_{EFx} + K_m} \tag{4}$$

with a maximum pump rate $V_{max} = 4$ mmol s^{-1} per liter of fiber volume and a Ca2+ concentration at which half-maximum pump rate is reached, $K_m = 0.5$ μM [5,29]. This implies that SERCA is active even in non-excited cells at rest. Therefore, a constant leak term in SERCA is included to keep $[Ca^{2+}]_{cyto}$ in quiescent cells constant.

This compartmental diffusional model extends the model proposed by Cannel and Allen [4] by including a more detailed geometry. In their model, as in other diffusional models [6–8,30,31], validation was only based on cytosolic Ca2+ transients. Our model validation is based on experimental data of free calcium concentration in SR and mitochondria, i.e. $[Ca^{2+}]_{SR}$, and $[Ca^{2+}]_{mito}$, respectively. In this comprehensive analysis, the diffusional approach which takes into account microdomains in the space adjacent to mitocondria or SR, becomes very important. This feature is absent in compartmental models which only consider averaged concentration within compartments.

The study of calcium dynamics in the mitochondrion is a relatively new subject [9,10,24,32–34]. However, a quantitative model of skeletal muscle fibers including mitochondria is still lacking. The governing equation for total Ca2+ concentration in the mitochondrion $[Ca^{2+}]_{mito,tot}$ is:

$$\frac{\partial[Ca^{2+}]_{mito,tot}}{\partial t} = J_{MCU}([Ca^{2+}]_{cyto}) - J_{NCE}([Ca^{2+}]_{mito}, [Ca^{2+}]_{cyto}) \tag{5}$$

J_{MCU} is the influx via the mitochondrial Ca2+ uniporter (MCU) and J_{NCE} is the efflux through mitochondrial Na+/Ca2+ exchanger (NCE). A detailed description of fluxes of Ca2+ ions through MCU, and NCE would require the analysis of all the components which influence the mitochondria membrane potential $\Delta\Psi_m$ which in turn affects MCU influx [35]. This would imply the analysis of $[H^+]$, $[Na^+]$, $[K^+]$, their flux through the inner mitochondrial membrane and relative buffers in the matrix, and would introduce several additional parameters to the model. We consider such a detailed description beyond the scope of the present work, and

adopt a simpler model based on a constant [Na$^+$] and a constant $\Delta\Psi_m$, which has proven to be suitable for cardiac myocytes, at relatively low frequency of stimulations [10]. In this approximation, J$_{MCU}$ is simplified as a saturable first-order transporter independent of the internal [Ca^{2+}]$_{mito}$:

$$J_{MCU} = J_{offset} + f_{MCU}V_{MCU}\frac{[Ca^{2+}]_x^h}{[Ca^{2+}]_x^h + K_d^h} \tag{6}$$

where V$_{MCU}$ is the maximum flux rate, [Ca^{2+}]$_x$ the Ca^{2+} concentration in the sub-compartments of EF where the mitochondrion resides and K$_d$ the Ca^{2+} concentration where the pump rate is half-maximal. f$_{MCU}$ is a multiplication factor to fit the data, h the Hill parameter and J$_{offset}$ the constant flux which equilibrates the basal flux via NCE, J$_{NCE}$.

J$_{NCE}$ is based on a 3:1 stoichiometry for Na$^+$ and Ca^{2+} [33], described with more detail in the S2 File, and contains a multiplicative factor f$_{NCE}$ with the same role as f$_{MCU}$. The equation used depends on the inner membrane potential $\Delta\Psi_m$, the cytosolic and intra-mitochondrial [Ca^{2+}] as well as cytosolic and intra-mitochondrial [Na$^+$]. This relationship leads to symmetrical uptake and decay transients in [Ca^{2+}]$_{mito}$. However, experimental data show that [Ca^{2+}]$_{mito}$ exhibits an average rise time during train of stimuli of 27.8 ms, much faster than its exponential decay after the end of stimulation (rate constant of 250 ms^{-1}). To account for this asymmetry, we propose a phenomenological modification of J$_{NCE}$, which follows the original description proposed in [33] up to [Ca^{2+}]$_{mito}$ = 1 µM, and increases exponentially above this value (see S2 File for an extended analysis and description).

Ca^{2+} buffers

The model includes the following Ca^{2+} buffers: Calsequestrin (CSQ) in the TC, an additional buffer (AB) in the SR, Parvalbumin (PVA) in cytosolic space (both EF and MS), Troponin C (Tn-C) in MS, and a buffer in the mitochondrial matrix (B). PVA-sites can be occupied also by Mg^{2+} whose concentration is assumed to be constant. Values for buffering capacity and binding and unbinding rates (reported in S1 Table) are assumed as in [5] for PVA (for Ca^{2+} and Mg^{2+}), and [7] for Tn-C (referring to fast-twitch mouse muscle), while tentative parameters for the mitochondrial buffer are taken from [10]. The cytosolic and mitochondrial buffers are considered to be uniformly distributed into the above-mentioned spaces and no cooperativity is assumed in the Ca^{2+}-binding process. Therefore, the governing equation is:

$$\frac{d[SCa^{2+}]}{dt} = k_{on}[Ca^{2+}][S] - k_{off}[SCa^{2+}] \tag{7}$$

where S and SCa^{2+} represent the free and calcium-bound form of the buffer, respectively. The previous equation should be applied to every sub-compartment in the cytosolic space, for every buffer S. However, the relative characteristic times for diffusion and binding events allow for a simplification which maintains the computation time suitable for a personal computer. The characteristic length for the diffusional event is about 1 µm, so using D = 300µm^{2}s^{-1} the characteristic time is τ_D = 3.3 ms. The calcium binding and release from troponin are the faster ones, because calcium binding to PVA is limited by the speed of Mg^{2+} release. However, in the presence of the highest [Ca^{2+}]$_{cyto}$ = 0.38 µM considered in this study, this event has a characteristic time of about τ_B = 30 ms, one order of magnitude higher than τ_D. We therefore introduced the simplification that, in each time step, the equilibrium between each buffer and the free calcium concentration is governed by the mean value of [Ca^{2+}] in the cytosolic space <[Ca^{2+}]$_{cyto}$> (see also [36]). In this case, the amount of calcium bound to or released from the

buffer S in each sub-compartment x, is proportional to the ratio $[Ca^{2+}]_x/<[Ca^{2+}]_{cyto}>$ and, only three PDEs, one for each cytosolic buffer, describe the binding kinetics.

The concentration of CSQ isoform 1 (CSQ1), the predominant form in rodent fast-twitch skeletal muscle, is equal to about 36 μmoles per liter of total fiber volume in rat muscle fibers with a binding capacity of up to 80 mol Ca²⁺ per mole of CSQ1 [37]. In the geometry used, corresponding to murine fibers, this leads to local concentration of 82.8 mM in TC. CSQ properties are modified from [4] to account for its cooperative buffering properties. A Hill equation for cooperative binding with a Hill coefficient of 3 was used, as determined for frog skeletal muscle [38]:

$$\frac{d[CSQCa^{2+}]}{dt} = k_{on}[Ca^{2+}]^3[CSQ] - k_{off}[CSQCa^{2+}] \qquad (8)$$

Eq 8 is a modified version of Eq 7 and includes the Hill coefficient as a power for the $[Ca^{2+}]$ in the right-hand-side. This introduces a reasonable approximation [39] compatible with the above-mentioned experimental data. The dissociation rate constant for CSQ was calculated from the binding rate constant in [5] and a level of 15% saturation of the total buffer capacity in quiescent fibers [40].

As to the additional buffers (AB) in the SR, a distinction has been made between linear and cooperative buffers [38]. Additional buffers are supposed to have a higher affinity but a several-fold lower capacity with respect of CSQ [41,42]. We used a Hill equation with h = 1, i.e. Eq 7, to describe the binding kinetics, with the appropriate slower rate constants. In an experimental work [38], best fitting of the experimental data was achieved using a ratio between the Ca²⁺ bound to AB and the Ca²⁺ bound to CSQ of approximately 0.1 at rest. We used this value, but also examined the effect of the maximum value of 0.2 estimated in [38].

The set of differential equations was solved using the ode15s built-in solver in MATLAB (The MathWorks Inc.). No external sources or drains are included, and the constancy of the total amount of Ca²⁺ at any time-step is used to test the reliability of the computations. Mass conservation is achieved within the limits of the software precision. Time steps are controlled by MATLAB; the validity of the results was tested using different values of absolute and relative tolerance (RelTol and AbsTol). Accuracy was tested using different initial conditions. Sensitivity analyses have been done for all the parameters used and are reported in S2 Table. Each parameter has been both increased and decreased by a 5%, while keeping other parameters constant, and the free calcium concentration in the three compartments have been compared to the values obtained in the basic WT model. Most of the modifications lead to a difference of less than 1%, and only the calsequestrin cooperativity lead to differences of more than 5%. Notably, 5% is less than the uncertainty or variability of parameters values as observed experimentally in different studies. However, the model has been compared against the data obtained in our laboratory with the same set-up and muscle type, on three compartments and for two different cell types (WT and CSQ-KO), supporting the validity of our conclusions. A more detailed analysis for mitochondrial buffering capacity and kinetics, as well as for the buffering capacity of AB, were done as described in the text and in the S3 and S4 Files.

Experimental data

[Ca²⁺] signals, i.e. variations in free calcium concentrations, adopted as reference for fitting, and simulation were derived from data previously published, using different ratiometric calcium probes in cytosol [16], SR [12], and mitochondria [13]. Single fibers were enzymatically dissociated from murine Flexor Digitorum Brevis muscle (FDB) and studied using an inverted fluorescence microscope at rest and during brief trains of stimulation at 1, 5, 20 and 60 Hz.

Cytosolic free Ca^{2+} determination was obtained loading fibers with Fura-2 acetoxymethyl ester and using a dual-beam excitation fluorescence photometry setup. Mitochondrial and SR free calcium concentrations were calculated from the single excitation, dual emission (YFP/CFP) intensity ratio after correction for background fluorescence. In these experiments, wild type (WT) mice and mice lacking both isoforms of Calsequestrin (CSQ-KO) were transfected with genetically targeted FRET-based indicators (Cameleons [43]) directed either to the SR (D1ER) or to the mitochondria (4mtD3cpv). An analysis of the ratiometric signal-calcium concentration relationship for Fura-2 and FRET based indicators (F-[Ca^{2+}] or R-[Ca^{2+}] respectively) has been derived in [30] and [14], which includes also a time dependent factor dF/dt and dR/dt to estimate the kinetics of binding and unbinding of the probes. Although no detailed information is available on the on-off kinetics of the D1ER and 4mtD3cpv, the experimental evidence [12,13] strongly support the view that these probes are sufficiently fast to record changes on a ms-time scale. The theoretical treatment and model simulations in S5 File support this view. All experimental data and, therefore, all simulations refer to a temperature of 25°C.

Results

Parameter fitting and model validation for wild type murine fast skeletal muscle fibers

a) Parameter fitting at 60 Hz stimulation. The numerical values of most parameters were taken from the literature, as described in the previous section. The value of P_{max} in Eq 3 was adjusted to match the experimental [Ca^{2+}]$_{cyto}$ recorded during a stimulation train at 60 Hz; the multiplicative parameters f_{MCU} and f_{NCE} and the parameters in J_{NCE} were adjusted to match the amplitude and time course of [Ca^{2+}]$_{mito}$ at 60 Hz (see Table 1). All other model parameters used are summarized in S1 Table.

In Fig 2 a comparison is shown between the time course of the model prediction and the typical experimental data (right and left columns respectively). The values of [Ca^{2+}] reported in Table 1 are extrapolated, on a relatively slow time scale (>10 ms), from the data reported in [12,13] considering the average value of the oscillations in [Ca^{2+}]$_{cyto}$ during the steady phase, as determined by measurements using Fura-2 and as proposed in [44], and the [Ca^{2+}] deduced by the change in the YFP/CFP ratio for SR and mitochondrion (see red lines in Fig 3, below).

Although the model is intended primarily to simulate the final steady state values of [Ca^{2+}] in the fiber compartments at 60 Hz stimulation, the kinetics of the recovery to quiescent steady state after stimulation trains are also in fair agreement with the experimental data. In particular, the asymmetry between the rising phase and the decay or recovery phase after the train of stimuli in the experimental [Ca^{2+}]$_{mito}$ (lower left panel of Fig 2) can be reproduced by the modification in J_{NCE} proposed in Methods and S2 File. Simulated recovery kinetics can be fitted by a single exponential, as in the experimental data, with rate constant $t_{SR} = 0.98$ s⁻¹ and $t_{mito} = 0.69$ s⁻¹, for SR and mitochondria respectively. The values are comparable to the corresponding experimental values of 0.3 s⁻¹ and 0.21 s⁻¹ [12,13].

Table 1. Experimental [Ca²⁺] in μM for WT muscle fibers. These values are averages measured at steady state during stimulation trains at various rates (60, 20, 5, and 1 Hz).

WT	60 Hz	20 Hz	5 Hz	1Hz
Cytosol	0.38	0.26	0.15	0.10
Mitochondrion	1.07	1.13	0.63	0.45
SR	362	452	446	470

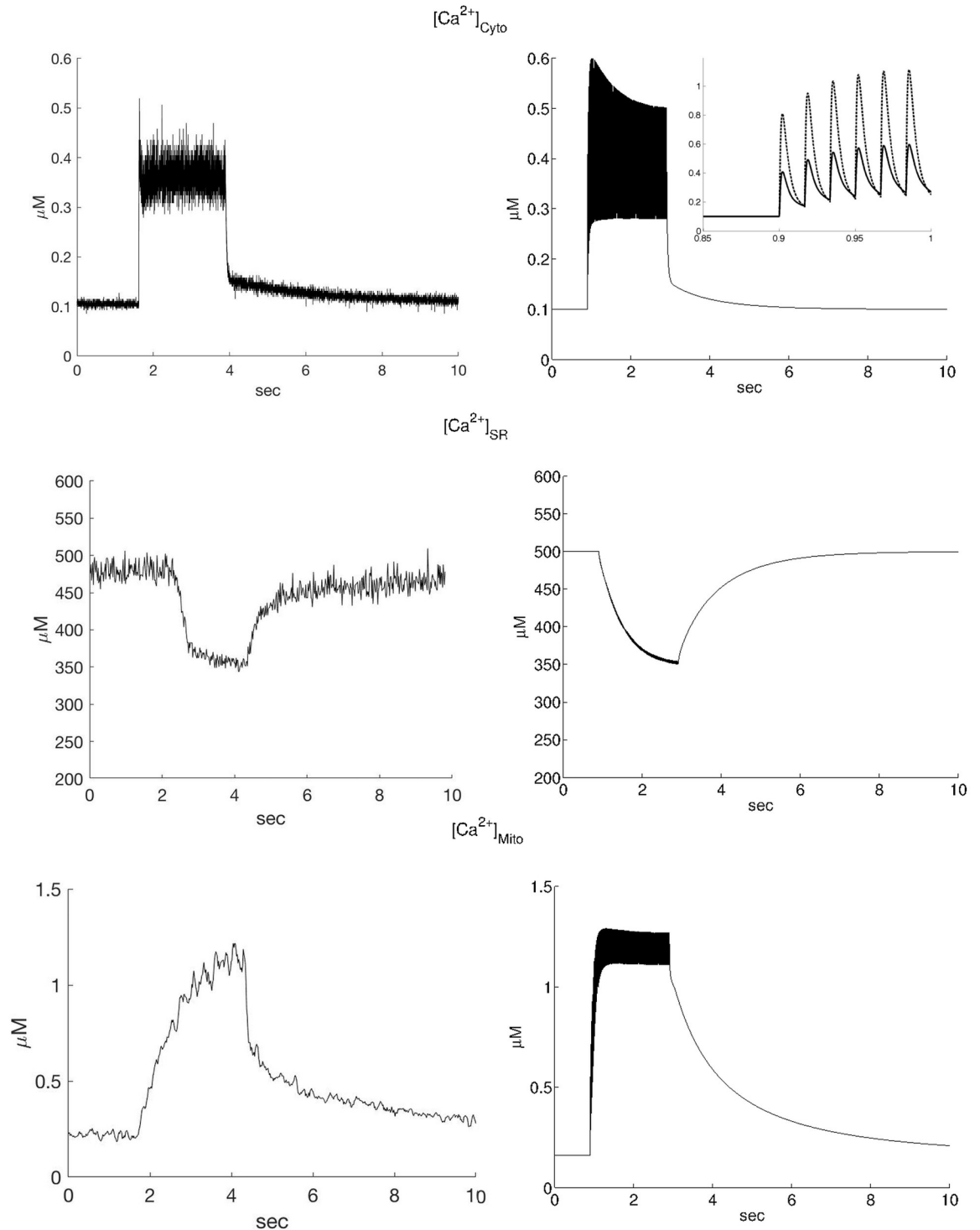https://doi.org/10.1371/journal.pone.0201050.t001

Fig 2. Experimental data and model simulations of calcium transients in a 2 s 60Hz stimulation train. Experimental data (left column, from [12] and [13] [Ca^{2+}] calculated from Fura 2 ratio and YFP/CFP ratios according to the equations reported in S5 File) and simulations (right column) of the [Ca^{2+}] transients in the cytosol (top), SR (middle) and mitochondrion (bottom) during a 2s stimulation train at 60 Hz. It can be seen that the steady-state values reached in the experiments agree well with the model simulations. In addition the time courses agree rather well considering that the model is based solely on previously published parameters. The amplitude of the oscillations in the model simulations are larger than in the experimental recordings, but this is as expected because the experimental recordings were smoothed by an x-point running average to reduce noise. In the inset of the cytosolic calcium simulation (top-right) the local Ca^{2+} concentration is shown (dotted line) in the element (microdomain) in front of MCU and NCE and compared

to the average cytosolic [Ca²⁺], showing an approximately two-fold increase. The lower-right panel shows the asymmetry in the rising phase (at the beginning of the train of stimuli), and at the decay phase (at the end of the train of stimuli) in the simulated mitochondrial [Ca²⁺].

https://doi.org/10.1371/journal.pone.0201050.g002

The inset in the upper right panel of Fig 2 shows the transient in [Ca²⁺] in the sub-compartment of the cytosolic space where the mitochondrion is located (top figure in the right panel, dotted trace). It can be seen that the local [Ca²⁺] is more than two-fold higher than the average [Ca²⁺]$_{cyto}$. This is in agreement with the concept of micro-domain [11] and stresses the importance of the diffusional approach followed.

b) Model validation by comparing the simulations at lower stimulation rates with the experimental recordings. The model with the parameters derived at 60 Hz stimulation was validated by considering the predictions of free calcium variations during stimulation at lower frequencies (1, 5 and 20 Hz). In Fig 4, the recorded and the predicted values are compared. The predicted values refer to the steady state condition reached at the end of the stimulation train and are denoted by the red lines in Fig 3. It can be seen that the steady state [Ca²⁺] values in all three compartments are in fair agreement with the experimental data at all stimulation rates. Simulated traces for [Ca²⁺] transients in the three compartments (cytosolic, mitochondrion and sarcoplasmic reticulum) at 1, 5 and 20 Hz stimulation and the analysis of the kinetics are reported in S3 and S6 Files.

Model prediction for muscle fibers of CSQ-KO mice

Next, given the long experience of our laboratories with mice carrying a null mutation of CSQ [12,13,45] we tested the ability of the model to predict the impact of ablation of CSQ without any other adaptive changes, except for the permeability parameter P$_{max}$, which was doubled to account for the increased number of RyRs, reported in [16]. Calcium can be bound by CSQ at the ratio 80 moles of calcium per 1 mole of CSQ [37], thus CSQ removal is expected to cause a marked reduction in calcium inside the SR [16], see Table 2. At high stimulation frequency, a reduction in calcium in the cytosol becomes evident; the free calcium concentration decreases after an initial peak since calcium is progressively taken up by PVA [12]. However, the drop in [Ca²⁺] is not as high as expected since the force generated is at least sufficient for normal mobility of sedentary mice.

The mechanisms behind these near-normal contractions are not well understood. The presence of other calcium buffering proteins in the SR, such as sarcalumenin, calreticulin, calnexin, junctate and others [42,46–49], could partially alleviate calcium shortage [50]. Without additional buffers, the model predicted a marked drop in [Ca²⁺] in all three compartments due to ablation of CSQ (data not shown). Results of the model with an additional buffer (AB) with a buffer capacity ratio relative to CSQ of 0.1 are reported in Fig 5 for the response to stimulation trains at 1 and 60 Hz, and are compared with experimental data in Fig 6 for the whole range of stimulation frequencies (1–60 Hz). As can be seen in Fig 5, the simulated [Ca²⁺]$_{cyto}$ has an initial peak similar to that predicted for WT, but it rapidly decreases to a lower steady value, while the [Ca²⁺]$_{SR}$ shows a much stronger depletion compared to WT. Qualitatively, these results resemble the behavior of free [Ca²⁺] in SR and cytosol in CSQ-KO cells [12]. Quantitatively, however, the model prediction for [Ca²⁺]$_{mito}$ is different from what is observed experimentally as [Ca²⁺]$_{mito}$ is not able to maintain the relatively high values observed in CSQ-KO, especially at high stimulation frequencies.

In an attempt to improve the prediction of [Ca²⁺]$_{mito}$ in CSQ-KO, we considered that doubling of the number of RyRs might lead to an increased RyR leakage in basal conditions. Since
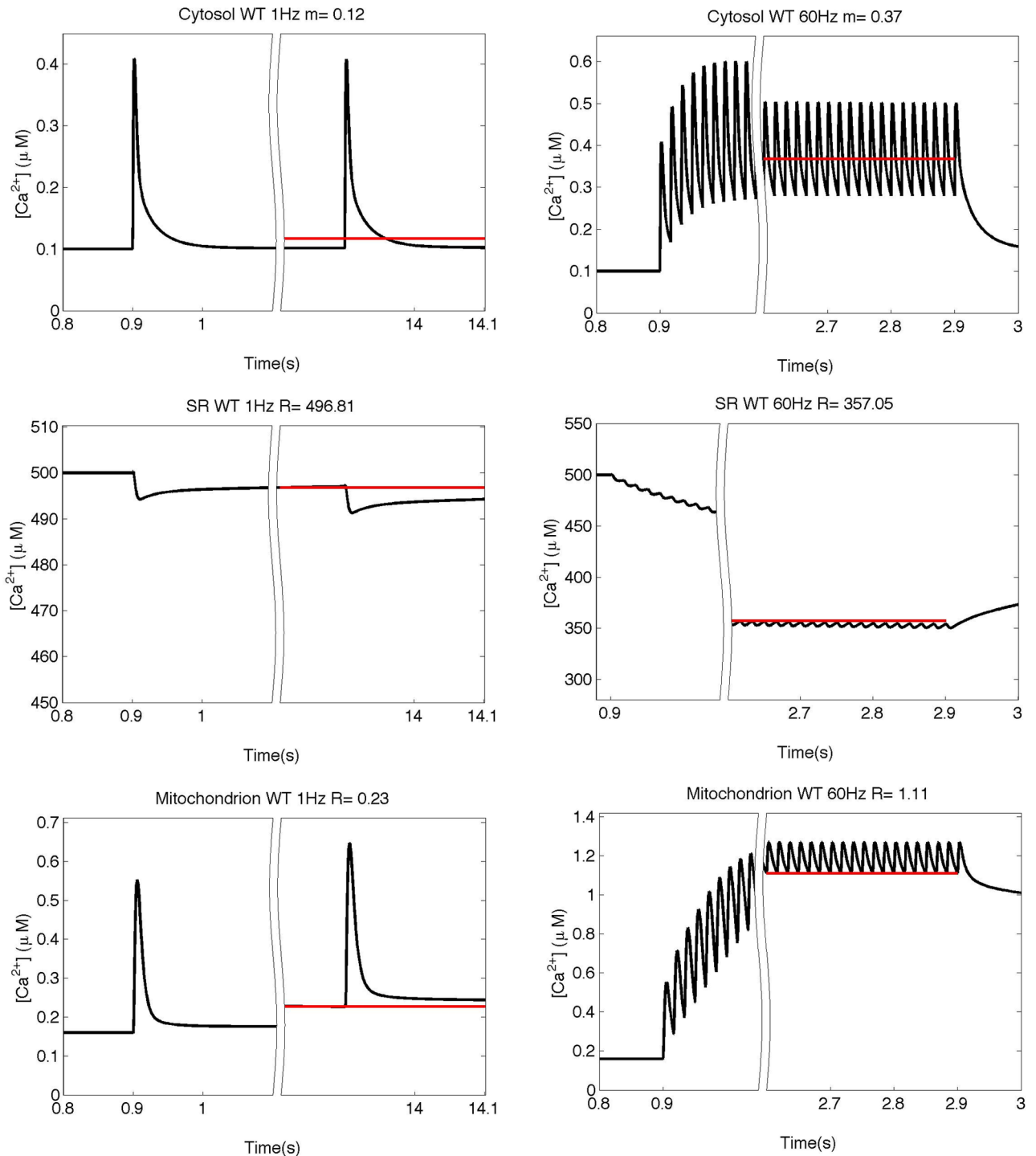
Fig 3. Simulation of the free calcium concentrations. Simulation of the free calcium concentrations in the three compartments at 1 and 60 Hz in the WT model at the beginning and at the end of the train of stimulation. Red lines represent the mean value ("m" for the cytosolic space) or the steady value before the beginning of the next stimulus ("s" in SR and mitochondrion). Above each panel the values for m or s are reported.
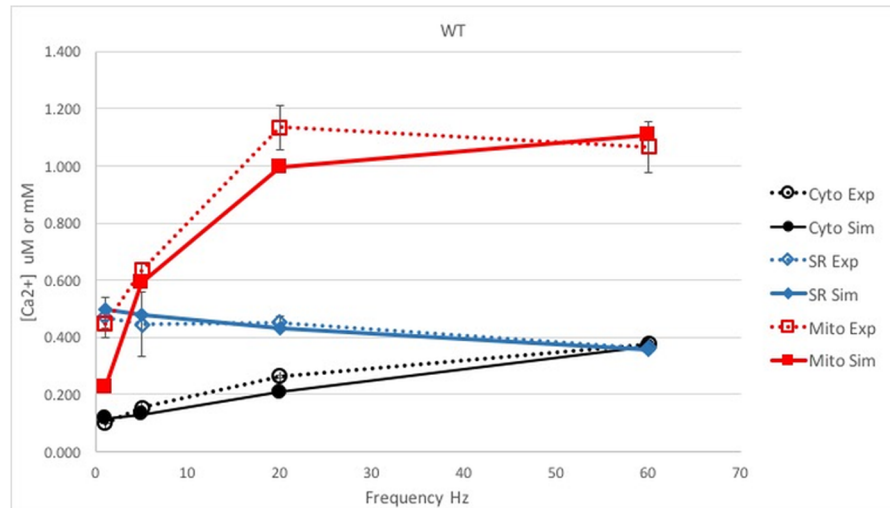
Fig 4. Comparison between the simulation and experiments in WT muscle fibers. The simulated [Ca^{2+}]reached at steady state in the three compartments and the experimental data for 1, 5, 20 and 60 Hz in WT mouse fibers are compared with experimental values. The free model parameters are adjusted to fit the data at 60 Hz. [Ca^{2+}] is reported in μM in cytosol or mitochondrion (black and red lines, respectively) or in mM for SR (blue line). Dotted lines: experimental data; continuous lines: model predictions.

https://doi.org/10.1371/journal.pone.0201050.g004

the basal [Ca^{2+}]$_{cyto}$ is the same in CSQ-KO and WT fibers, SERCA needs to pump twice as much. This will lead to a constant average [Ca^{2+}]$_{cyto}$, but higher local concentrations near the RyR. In principle, the higher local [Ca^{2+}]$_{cyto}$ might allow for the observed higher basal [Ca^{2+}]$_{mito}$ (230 nM in CSQ-KO vs 160 nM in WT [13]) because of the proximity of the mitochondrion to the sites of release. However, the increase predicted after doubling of the number of RyRs is clearly insufficient, since it increased the basal [Ca^{2+}]$_{mito}$ by less than 1%.

In a further attempt to improve the simulated calcium kinetics in CSQ-KO fibers, we considered an increase in the additional buffer capacity inside SR. An estimate of the relative amount of Ca^{2+} bound to CSQ and secondary additional buffers with linear properties has been made in frog skeletal muscles [38]. In that study, the maximum limit of Ca^{2+} bound to the secondary buffer was inferred to be 20% of total calcium bound in the sarcoplasmic reticulum at rest. In our simulations, if 20% of total SR calcium is bound to AB, [Ca^{2+}]$_{cyto}$ at 60 Hz is close to the experimental data in CSQ-KO (see Fig 7). However, Table 3 illustrates that the predicted values of free calcium in the SR ([Ca^{2+}]$_{SR}$) during 60 Hz stimulation would be lower than those observed experimentally (predicted/experimental ratio = 0.86), indicating that even in this extreme case the effect of the AB is insufficient to sustain the near-normal contraction at high frequencies. Thus, the model suggests that an extra source of external calcium (possibly via SOCE) is needed as hypothesized in [12] and recently discussed in [45].

Table 2. Experimental average [Ca^{2+}] in μM for CSQ-KO mouse muscle fibers measured in the steady state attained during stimulation trains at various rates (1, 5, 20, 60 Hz).

		60 Hz	20 Hz	5 Hz	1Hz
CSQ-KO	Cyto (μM)	0.18	0.18	0.14	0.10
	Mito (μM)	0.74	0.73	0.62	0.43
	SR (μM)	104	177	302	440

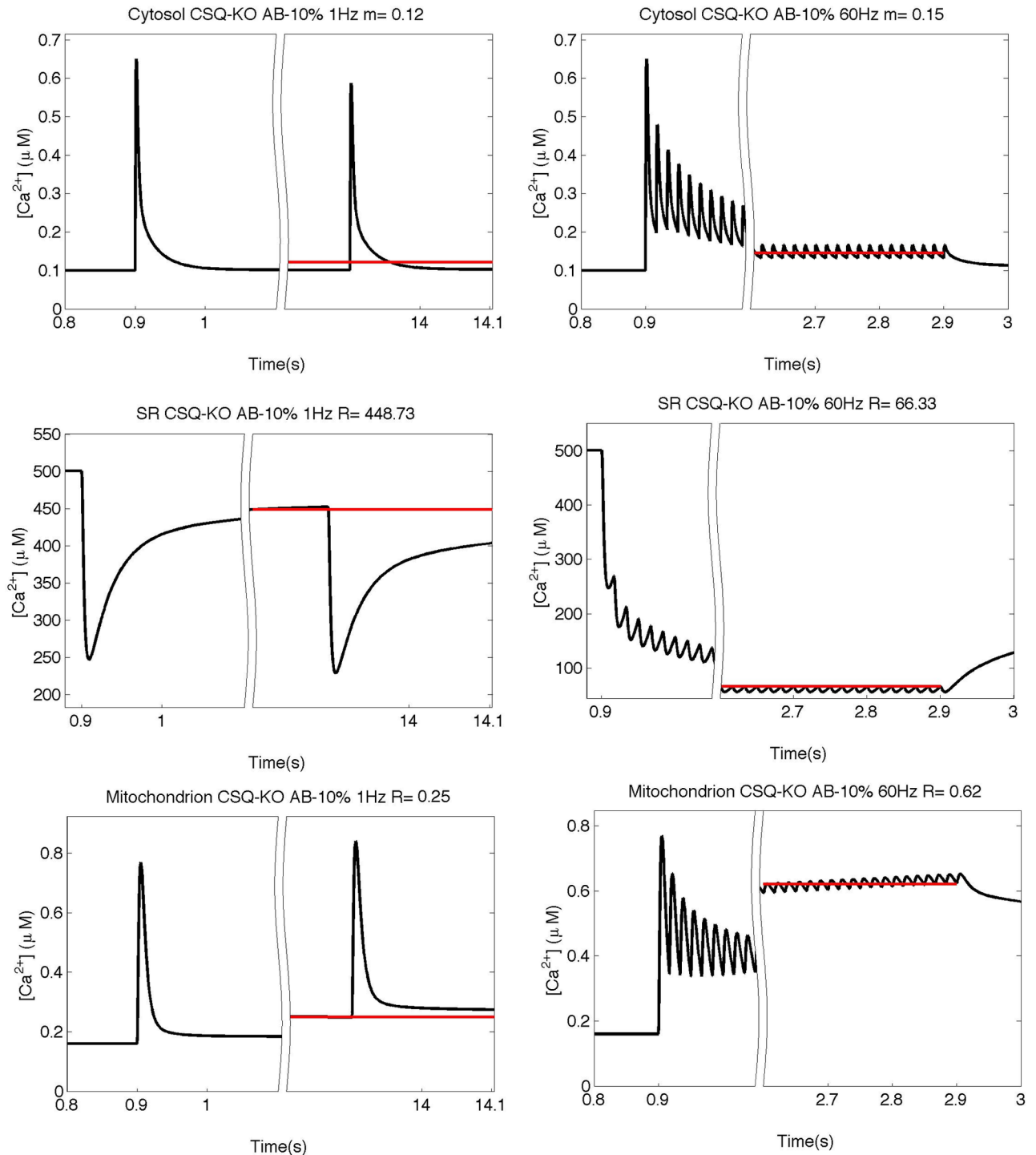https://doi.org/10.1371/journal.pone.0201050.t002

Fig 5. Simulation of the free calcium concentrations in CSQ-KO with an AB buffering capacity of 10% of that of CSQ. Simulation of the free calcium concentrations in the three compartments at 1 and 60 Hz as predicted by the model without CSQ (CSQ-KO) with a AB buffering capacity of 10% of that of CSQ and with doubled P_{max} value. Red lines represent the mean value ("m" for the cytosolic space) or the steady value before the beginning of the next stimulus ("s" in SR and mitochondrion). Above each panel the values for m or s are reported.
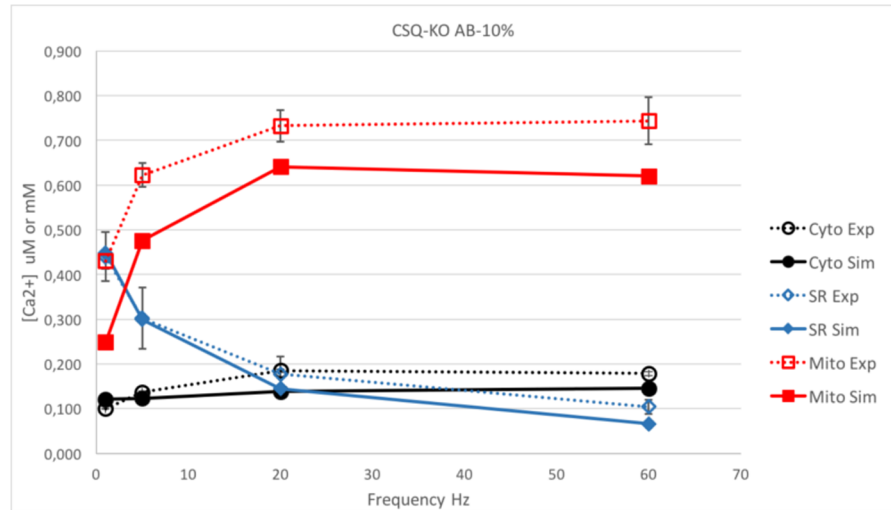
Fig 6. Comparison between the simulation and experiments in CSQ-KO with an AB buffering capacity of 10% of that of CSQ. Comparison between the simulated steady state [Ca²⁺] in the three compartments and the experimental data for 1, 5, 20 and 60 Hz in CSQ-KO mouse with 10% of total calcium bound in the SR at rest accounted by AB and with doubled Pmax value. [Ca²⁺] is reported in µM in cytosol or mitochondrion (black and red lines, respectively) or in mM for SR (blue line). Dotted lines stand for experimental data, continuous lines for simulations. The model without CSQ (CSQ-KO), with 10% of AB capacity and double Pmax fails to match the observed values in all three compartments, with predicted values lower than experimental data.

https://doi.org/10.1371/journal.pone.0201050.g006

Discussion and conclusions

In this study, we designed a new model to reproduce the Ca²⁺ dynamics in skeletal muscle fibers of WT mice. The model is based on previously published models which account for
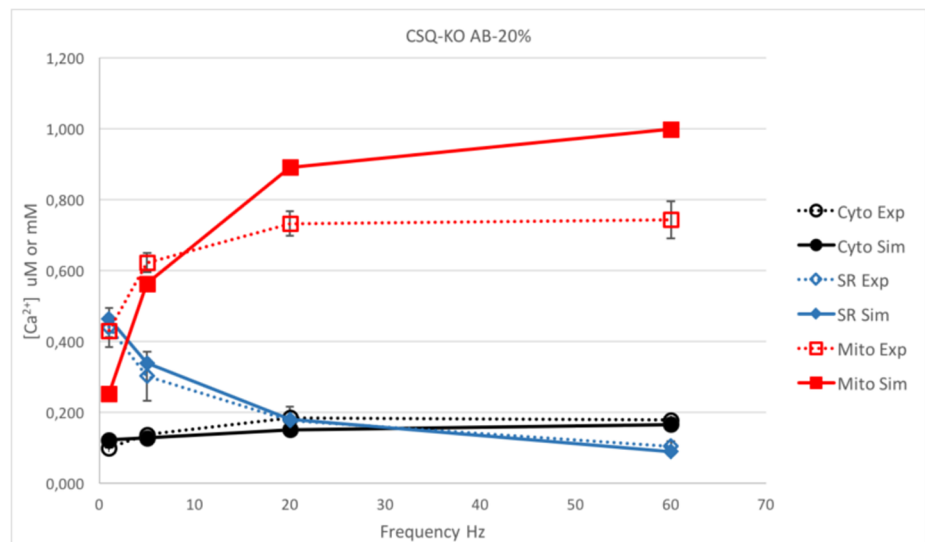

Fig 7. Comparison between the simulation and experiments in CSQ-KO with an AB buffering capacity of 20% of that of CSQ. Comparison between the simulated steady state [Ca²⁺] in the three compartments and the experimental data for 1, 5, 20 and 60 Hz in CSQ-KO mouse with increased AB buffering to 20% of the capacity of CSQ. [Ca²⁺] is reported in µM in cytosol or mitochondrion (black and red lines, respectively) or in mM for SR (blue line). Dotted lines stand for experimental data, continuous lines for simulations.

https://doi.org/10.1371/journal.pone.0201050.g007

Table 3. Simulated/Experimental ratio for [Ca²⁺] in µM for WT and CSQ-KO fibers, assuming the amount bound by secondary buffer capacity at 10% or at 20%. The values are calculated at the steady state during the trains of stimulations, as in the Figs 3, 6 and 7.

		60 Hz	20 Hz	5 Hz	1Hz
WT 10%	Cyto	0.98	0.79	0.84	1.17
	Mito	1.04	0.88	0.94	0.51
	SR	0.99	0.95	1.08	1.06
CSQ-KO 10%	Cyto	0.81	0.75	0.90	1.21
	Mito	0.83	0.88	0.76	0.58
	SR	0.64	0.82	0.99	1.02
CSQ-KO 20%	Cyto	0.93	0.82	0.93	1.22
	Mito	1.34	1.22	0.90	0.59
	SR	0.86	1.02	1.12	1.06

https://doi.org/10.1371/journal.pone.0201050.t003

different intracellular compartments as well as for Ca²⁺ diffusion [4,7]. Compared to previous diffusional models, this is the first to take into consideration the three main compartments (cytosol, SR and mitochondria), and the first to be validated against a comprehensive set of experimental data on Ca²⁺ concentrations measured in these three compartments in murine muscle fibers. The numerical values of the parameters adopted in this study largely correspond to literature data. When data for mouse were not available, we adopted values from other studies as initial guesses and analyzed the effects of their variability (S2 Table). This was the case for the mitochondrial buffer and additional buffer in the SR.

A strong feature, illustrating the robustness of the model, is that only few parameters have been derived by fitting the model prediction to experimental data. These are: P_{max}, used to match the transient variations in $[Ca^{2+}]_{cyto}$ upon electrical stimulation; f_{MCU} and f_{NCE}, as well as the parameters for the exponential increase in J_{NCE}, $[Ca^{2+}]_{th}$ and γ (see S2 File), used to mimic the transients in the rise and decay phases of the $[Ca^{2+}]_{mito}$. The fitting was based on the Ca²⁺ concentrations recorded during a stimulation train at 60 Hz, and the results were validated as they provided a very good prediction for the Ca²⁺ concentration variations at lower stimulation frequencies (1, 5 and 20 Hz) in all three compartments. The model was then applied to predict the free calcium concentrations in the three compartments of muscle fibers devoid of CSQ (CSQ-KO). These results provided an additional test of the model and allowed us to estimate the impact of an additional buffer inside the SR.

The results showed that even the maximal buffer capacity of a secondary buffer (AB) accounting for 20% of the buffering power of CSQ in WT fibers [38] was insufficient to explain the data and this lends support for the hypothesis that external influx via SOCE would be required to account for the missing Ca²⁺. Interestingly, fast recruitment of SOCE has been shown in CSQ-KO myotubes [51]. A recent study [52] suggests that in skeletal muscle SOCE occurs in close spatial relation with the SR Ca²⁺-pumps, in specialized structures extending from the triad toward the Z-line, as schematically indicated in Fig 1. In this situation, free $[Ca^{2+}]_{SR}$ would be influenced by the SR buffer capacity and external Ca²⁺-influx via SOCE. As a consequence, the total Ca²⁺ within the fibers would increase and the calcium entry during one contractile cycle should benefit the subsequent one, as extrusion of the Ca²⁺ from the fibers is expected to occur more slowly than entry via SOCE.

An estimate of the extra amount of calcium needed to reproduce the experimental data in CSQ-KO fibers can be obtained as follow. In the model simulation of a short (2 s) stimulation train at 60 Hz in WT muscle fibers, approximately 260 µM of calcium (or 260 µmoles/liter fiber) move from the SR to the cytosol, 250 µM derived from CSQ and 10 µM from AB which

has a higher affinity and a lower capacity compared to CSQ. When CSQ is absent, the contribution of AB in the model rises in the extreme case to c.a. 60 μM in direct relation to the lowering of the [Ca^{2+}]$_{SR}$. Such an amount is well below what is required to keep cytosolic levels comparable not only to those of WT muscle fibers (approximately 180 μM would be needed in addition) but also to those experimentally observed in CSQ muscles (a contribution in the order of 100 μM would be required). This latter value corresponds (within 2 s) with a flux of 50 μM/s which is, in view of the uncertainties in the experimental determinations and in the calculations, in fair agreement with the experimentally estimated value of SOCE of 19 μM/s in [53].

The inclusion of mitochondrial calcium handling in the model represents a novelty for skeletal muscle fibers. Compared to other cell types, the volume occupied by mitochondria in skeletal muscle fibers is relatively small (approximately 5% vs. 30% in cardiomyocytes), and its contribution to Ca^{2+} homeostasis has been generally neglected (see [7]). Their localization in close proximity to the CRUs, which allows mitochondria to exploit Ca^{2+} microdomains [11] and the presence of specific components of the MCU, as for example MICU1.1 [54] which enhances Ca^{2+} transport, opens to the possibility that the amount of Ca^{2+} taken up by the mitochondria is greater than previously predicted. In addition, being close to TC and T-tubules the mitochondria might become a reliable indicator of the amount of Ca^{2+} released by RyR channels, if properly modeled.

These considerations prompted us to introduce mitochondria in the model. However, quantitative description of the mitochondrial Ca^{2+} kinetics is not an easy task. Three processes need to be considered: uptake by MCU, buffering, and release via NCE. In the last decades, several studies have proposed models of these three processes, mostly with reference to cardiomyocytes [9,24,33,34,55]. At the same time, probes for measuring intra-mitochondrial calcium concentrations have been developed and one of them (cameleon 4mtD3cpv) has been used to obtain the data analyzed in this study [13]. Considering that the aim of the present study was to provide an overall global quantitative simulation of Ca^{2+} dynamics in skeletal muscle fibers, several simplifications of the three processes (uptake-buffering-release) were introduced. Such simplifications proved to be suitable to simulate free calcium variations in the mitochondrial matrix, at rest and during trains of stimuli, in WT and CSQ-KO fibers. Our model of mitochondria was able to account for a number of observed behaviors, including the asymmetry of mitochondrial Ca^{2+} uptake and release. The emerging picture is that mitochondria take up a minor amount of calcium, thus confirming previous notions discussed in [13].

It is important to recall that the model has several limitations:

1. The model does not include the Ca^{2+}-dependent inactivation (CDI), i.e. the reduction in RyR permeability during a train of APs due to the increased Ca^{2+} concentration on the cytosolic side of RyR [7]. However, as shown in S1 File, we tested the CDI effect adopting an exponential decay of P$_{max}$ in accordance to [7]. The impact of such variation in permeability is well visible in the first stimuli of a train, but becomes rather small in the stimulation trains lasting for 1 or more seconds.

2. It is known that SERCA activity is cooperative and models are available to account for this, for example [5,56]. For the sake of simplicity we followed the proposal (see [4]) that the behavior of the pump could be simulated by Michelis-Menten kinetics, paying due attention to the choice of the values of K$_m$ and V$_{max}$.

3. The simulation of the calcium uptake via MCU and release via NCE could be improved by taking the influence of Na$^+$ and H$^+$ homeostasis and ΔΨ$_m$ into account, as suggested by our modification of the dependency of J$_{NCE}$ on [Ca^{2+}]$_{mito}$. These aspects warrant further study because quantitative data on mitochondria in living skeletal muscle fibers are still scarce.

In conclusion, the present model is implemented on a robust background dating back 30 years ago [4,6], but represents a significant improvement as it is the first to take into account all three major compartments, cytosol, SR lumen and mitochondrial matrix, and is validated by experimental data on calcium dynamics at rest and during trains of stimuli in all three compartments in skeletal muscle. The model has been tested in its ability to predict the calcium dynamics in CSQ-KO muscle fibers. The choice of this particular transgenic model was inspired by the specific experience of our laboratories [12,13,16,45], but also by the special relevance of this protein in the derailment of calcium kinetics in muscle disorders. Beside these specific results, the test on CSQ-KO muscle fibers illustrates the predictive ability of the model and its power to interpret and predict experimental results. Our model thus has the potential to be a helpful tool in the quantitative analyses of alterations of calcium dynamics in muscle fibers of genetically modified mice strains and to further study the impact of interventions, such as protein ablations or pharmacological treatments, on intracellular calcium dynamics.

Supporting information

S1 Table. Parameters definitions and values.
(PDF)

S2 Table. Sensitivity analysis. To evaluate the sensitivity of the model predictions on the actual model parameters, a change of ±5% has been applied to each parameter reported in Table 2, relative to the value given in Table 1. The variations of free [Ca²⁺] in the three compartments (cytosol, SR, mitochondrion) using these modified parameters ([Ca²⁺]±5%) relative to the values obtained with the parameter values in Table 1 ([Ca²⁺]basic) are calculated and expressed as a percentage (-5%/+5%). All percentages are lower than 5% except for the Hill parameter (an exponential term) in the calsequestrin equilibrium equation. The values of $100 \cdot \left(\frac{[Ca^{2+}]_{5\%}}{[Ca^{2+}]_{basic}} - 1 \right)$ in the three compartments are reported. "-"means less than 0.1% deviation. Values are given for the -5%/+5% cases.
(PDF)

S1 Fig. Effect of the compartment dimension. Simulation of the [Ca²⁺] in the cytosol where NCE and MCU are supposed to be located (125 nm away from the RyR) and in the mitochondrion using the 50-compartments model (red) and a 300-compartments model (blue).
(PDF)

S1 File. Ca²⁺-dependent inactivation of SR Ca²⁺-release. Effect of the Ca²⁺ dependent inactivation on the model prediction.
(PDF)

S2 File. Mitochondrion modeling. Equations for the MCU and NCE fluxes in mitochondrion and phenomenological hypothesis.
(PDF)

S3 File. Analysis of the kinetics of the decay phase of the transients in sarcoplasmic reticulum and mitochondrion. Although the model was designed mainly to simulate the steady state concentrations reached at rest or during stimulation trains in the three main compartments, also the kinetics after the train of stimuli were well simulated, both in SR and in mitochondrion.
(PDF)

S4 File. Sensitivity analysis of the mitochondrial buffer parameters. The nature of the mitochondrial buffer is largely unknown at present, and experimental data needed for its mathematical characterization are not available in literature. We have analyzed the $[Ca^{2+}]_{mito}$ behavior for different choices of the buffering capacity and kinetics, keeping a ratio for free-to-bound $[Ca^{2+}]$ of 1:100.
(PDF)

S5 File. Kinetics and steady state determination of Ca2+ concentrations. Effect of the kinetic term on the $[Ca^{2+}]$ in the three compartments.
(PDF)

S6 File. Time course of the variations in free $[Ca^{2+}]$ for the three compartments. Time course of the variations in free $[Ca^{2+}]$ for the three compartments at different stimulation rates in WT fibers and CSQ-KO fibers with 10% and 20% of total calcium bound accounted by secondary buffer LB.
(PDF)

S1 Video. Intracellular dynamics of the $[Ca^{2+}]_{cyto}$ during the steady state phase of a train of stimuli at 60 Hz frequency in the wild type model. The peak corresponds to the position of the ryanodine receptors.
(AVI)

Author Contributions

Conceptualization: Lorenzo Marcucci, Ger J. M. Stienen, Carlo Reggiani.

Data curation: Lorenzo Marcucci, Marta Canato, Feliciano Protasi, Carlo Reggiani.

Formal analysis: Lorenzo Marcucci, Ger J. M. Stienen, Carlo Reggiani.

Investigation: Lorenzo Marcucci, Carlo Reggiani.

Methodology: Lorenzo Marcucci, Ger J. M. Stienen, Carlo Reggiani.

Software: Lorenzo Marcucci.

Validation: Lorenzo Marcucci, Ger J. M. Stienen, Carlo Reggiani.

Visualization: Lorenzo Marcucci, Carlo Reggiani.

Writing – original draft: Lorenzo Marcucci, Marta Canato, Feliciano Protasi, Ger J. M. Stienen, Carlo Reggiani.

References

1. Gordon AM, Homsher E, Regnier M. Regulation of Contraction in Striated Muscle. Physiol Rev. 2000; 80: 853–924. https://doi.org/10.1152/physrev.2000.80.2.853 PMID: 10747208

2. MacLennan DH, Zvaritch E. Mechanistic models for muscle diseases and disorders originating in the sarcoplasmic reticulum. Biochim Biophys Acta BBA—Mol Cell Res. 2011; 1813: 948–964. https://doi.org/10.1016/j.bbamcr.2010.11.009 PMID: 21118704

3. Ríos E, Figueroa L, Manno C, Kraeva N, Riazi S. The couplonopathies: A comparative approach to a class of diseases of skeletal and cardiac muscle. J Gen Physiol. 2015; 145: 459–474. https://doi.org/10.1085/jgp.201411321 PMID: 26009541

4. Cannell MB, Allen DG. Model of calcium movements during activation in the sarcomere of frog skeletal muscle. Biophys J. 1984; 45: 913–925. https://doi.org/10.1016/S0006-3495(84)84238-1 PMID: 6733242

5. Westerblad H, Allen DG. The role of sarcoplasmic reticulum in relaxation of mouse muscle; effects of 2, 5-di (tert-butyl)-1, 4-benzohydroquinone. J Physiol. 1994; 474: 291. PMID: 8006816

6. Baylor SM, Hollingworth S. Model of Sarcomeric Ca2+ Movements, Including ATP Ca2+ Binding and Diffusion, during Activation of Frog Skeletal Muscle. J Gen Physiol. 1998; 112: 297–316. PMID: 9725890

7. Baylor SM, Hollingworth S. Simulation of Ca ²⁺ Movements within the Sarcomere of Fast-Twitch Mouse Fibers Stimulated by Action Potentials. J Gen Physiol. 2007; 130: 283–302. https://doi.org/10.1085/jgp.200709827 PMID: 17724162

8. Hollingworth S, Kim MM, Baylor SM. Measurement and simulation of myoplasmic calcium transients in mouse slow-twitch muscle fibres: Calcium movements in slow-twitch fibres. J Physiol. 2012; 590: 575–594. https://doi.org/10.1113/jphysiol.2011.220780 PMID: 22124146

9. Hatano A, Okada J, Washio T, Hisada T, Sugiura S. A Three-Dimensional Simulation Model of Cardiomyocyte Integrating Excitation-Contraction Coupling and Metabolism. Biophys J. 2011; 101: 2601–2610. https://doi.org/10.1016/j.bpj.2011.10.020 PMID: 22261047

10. Wüst RCI, Helmes M, Martin JL, van der Wardt TJT, Musters RJP, van der Velden J, et al. Rapid frequency-dependent changes in free mitochondrial calcium concentration in rat cardiac myocytes: Mitochondrial calcium handling. J Physiol. 2017; 595: 2001–2019. https://doi.org/10.1113/JP273589 PMID: 28028811

11. Rizzuto R, Pozzan T. Microdomains of Intracellular Ca2+: Molecular Determinants and Functional Consequences. Physiol Rev. 2006; 86: 369–408. https://doi.org/10.1152/physrev.00004.2005 PMID: 16371601

12. Canato M, Scorzeto M, Giacomello M, Protasi F, Reggiani C, Stienen GJM. Massive alterations of sarcoplasmic reticulum free calcium in skeletal muscle fibers lacking calsequestrin revealed by a genetically encoded probe. Proc Natl Acad Sci. 2010; 107: 22326–22331. https://doi.org/10.1073/pnas.1009168108 PMID: 21135222

13. Scorzeto M, Giacomello M, Toniolo L, Canato M, Blaauw B, Paolini C, et al. Mitochondrial Ca2+-Handling in Fast Skeletal Muscle Fibers from Wild Type and Calsequestrin-Null Mice. Kanzaki M, editor. PLoS ONE. 2013; 8: e74919. https://doi.org/10.1371/journal.pone.0074919 PMID: 24098358

14. Sztretye M, Yi J, Figueroa L, Zhou J, Royer L, Allen P, et al. Measurement of RyR permeability reveals a role of calsequestrin in termination of SR Ca2+ release in skeletal muscle. J Gen Physiol. 2011; 138: 231–247. https://doi.org/10.1085/jgp.201010592 PMID: 21788611

15. Royer L, Sztretye M, Manno C, Pouvreau S, Zhou J, Knollmann BC, et al. Paradoxical buffering of calcium by calsequestrin demonstrated for the calcium store of skeletal muscle. J Gen Physiol. 2010; 136: 325–338. https://doi.org/10.1085/jgp.201010454 PMID: 20713548

16. Paolini C, Quarta M, Nori A, Boncompagni S, Canato M, Volpe P, et al. Reorganized stores and impaired calcium handling in skeletal muscle of mice lacking calsequestrin-1: Calsequestrin role in skeletal muscle. J Physiol. 2007; 583: 767–784. https://doi.org/10.1113/jphysiol.2007.138024 PMID: 17627988

17. Dainese M, Quarta M, Lyfenko AD, Paolini C, Canato M, Reggiani C, et al. Anesthetic- and heat-induced sudden death in calsequestrin-1-knockout mice. FASEB J. 2009; 23: 1710–1720. https://doi.org/10.1096/fj.08-121335 PMID: 19237502

18. Protasi F, Paolini C, Dainese M. Calsequestrin-1: a new candidate gene for malignant hyperthermia and exertional/environmental heat stroke. J Physiol. 2009; 587: 3095–3100. https://doi.org/10.1113/jphysiol.2009.171967 PMID: 19417098

19. Paolini C, Quarta M, D'Onofrio L, Reggiani C, Protasi F. Differential effect of calsequestrin ablation on structure and function of fast and slow skeletal muscle fibers. J Biomed Biotechnol. 2011; 2011: 634075. https://doi.org/10.1155/2011/634075 PMID: 21941434

20. Protasi F, Paolini C, Canato M, Reggiani C, Quarta M. Lessons from calsequestrin-1 ablation in vivo: much more than a Ca(2+) buffer after all. J Muscle Res Cell Motil. 2011; 32: 257–270. https://doi.org/10.1007/s10974-011-9277-2 PMID: 22130610

21. Tomasi M, Canato M, Paolini C, Dainese M, Reggiani C, Volpe P, et al. Calsequestrin (CASQ1) rescues function and structure of calcium release units in skeletal muscles of CASQ1-null mice. AJP Cell Physiol. 2012; 302: C575–C586. https://doi.org/10.1152/ajpcell.00119.2011 PMID: 22049211

22. Mobley BA, Eisenberg BR. Sizes of components in frog skeletal muscle measured by methods of stereology. J Gen Physiol. 1975; 66: 31–45. PMID: 1159401

23. Luff AR, Atwood HL. Changes in the sarcoplasmic reticulum and transverse tubular system of fast and slow skeletal muscles of the mouse during postnatal development. J Cell Biol. 1971; 51: 369–383. PMID: 5112650

24. Williams GSB, Boyman L, Chikando AC, Khairallah RJ, Lederer WJ. Mitochondrial calcium uptake. Proc Natl Acad Sci. 2013; 110: 10479–10486. https://doi.org/10.1073/pnas.1300410110 PMID: 23759742

25. Boncompagni S, Rossi AE, Micaroni M, Beznoussenko GV, Polishchuk RS, Dirksen RT, et al. Mito-chondria are linked to calcium stores in striated muscle by developmentally regulated tethering struc-tures. Mol Biol Cell. 2009; 20: 1058–1067. https://doi.org/10.1091/mbc.E08-07-0783 PMID: 19037102

26. Hollingworth S, Soeller C, Baylor SM, Cannell MB. Sarcomeric Ca2+ gradients during activation of frog skeletal muscle fibres imaged with confocal and two-photon microscopy. J Physiol. 2000; 526: 551–560. https://doi.org/10.1111/j.1469-7793.2000.t01-1-00551.x PMID: 10922007

27. Crank J. The Mathematics of Diffusion. Clarendon Press; 1979.

28. Royer L, Pouvreau S, Ríos E. Evolution and modulation of intracellular calcium release during long-last-ing, depleting depolarization in mouse muscle: Calcium flux and depletion in muscle. J Physiol. 2008; 586: 4609–4629. https://doi.org/10.1113/jphysiol.2008.157990 PMID: 18687715

29. Lytton J, Westlin M, Burk SE, Shull GE, MacLennan DH. Functional comparisons between isoforms of the sarcoplasmic or endoplasmic reticulum family of calcium pumps. J Biol Chem. 1992; 267: 14483–14489. PMID: 1385815

30. Jiang Y-H, Klein MG, Schneider MF. Numerical Simulation of Ca2+?Sparks? in Skeletal Muscle. Bio-phys J. 1999; 77: 2333–2357. https://doi.org/10.1016/S0006-3495(99)77072-4 PMID: 10545338

31. Novo D, DiFranco M, Vergara JL. Comparison between the Predictions of Diffusion-Reaction Models and Localized Ca2+ Transients in Amphibian Skeletal Muscle Fibers. Biophys J. 2003; 85: 1080–1097. https://doi.org/10.1016/S0006-3495(03)74546-9 PMID: 12885654

32. Cortassa S, Aon MA, O'Rourke B, Jacques R, Tseng H-J, Marbán E, et al. A Computational Model Inte-grating Electrophysiology, Contraction, and Mitochondrial Bioenergetics in the Ventricular Myocyte. Bio-phys J. 2006; 91: 1564–1589. https://doi.org/10.1529/biophysj.105.076174 PMID: 16679365

33. Dash RK, Beard DA. Analysis of cardiac mitochondrial Na $^+$ -Ca $^{2+}$ exchanger kinetics with a biophysical model of mitochondrial Ca $^{2+}$ handing suggests a 3: 1 stoichiometry: Characterization of mitochondrial NCE stoichiometry. J Physiol. 2008; 586: 3267–3285. https://doi.org/10.1113/jphysiol.2008.151977 PMID: 18467367

34. Boyman L, Chikando AC, Williams GSB, Khairallah RJ, Kettlewell S, Ward CW, et al. Calcium Move-ment in Cardiac Mitochondria. Biophys J. 2014; 107: 1289–1301. https://doi.org/10.1016/j.bpj.2014.07.045 PMID: 25229137

35. Gunter TE, Pfeiffer DR. Mechanisms by which mitochondria transport calcium. Am J Physiol-Cell Phy-siol. 1990; 258: C755–C786.

36. Wagner J, Keizer J. Effects of rapid buffers on Ca2+ diffusion and Ca2+ oscillations. Biophys J. 1994; 67: 447–456. https://doi.org/10.1016/S0006-3495(94)80500-4 PMID: 7919018

37. Murphy RM, Larkins NT, Mollica JP, Beard NA, Lamb GD. Calsequestrin content and SERCA deter-mine normal and maximal Ca $^{2+}$ storage levels in sarcoplasmic reticulum of fast- and slow-twitch fibres of rat: Calsequestrin and SR Ca $^{2+}$ content in single muscle fibres. J Physiol. 2009; 587: 443–460. https://doi.org/10.1113/jphysiol.2008.163162 PMID: 19029185

38. Fénelon K, Lamboley CRH, Carrier N, Pape PC. Calcium buffering properties of sarcoplasmic reticulum and calcium-induced Ca2+ release during the quasi-steady level of release in twitch fibers from frog skeletal muscle. J Gen Physiol. 2012; 140: 403–419. https://doi.org/10.1085/jgp.201110730 PMID: 23008434

39. Weiss JN. The Hill equation revisited: uses and misuses. FASEB J Off Publ Fed Am Soc Exp Biol. 1997; 11: 835–841.

40. Park H, Park IY, Kim E, Youn B, Fields K, Dunker AK, et al. Comparing skeletal and cardiac calseques-trin structures and their calcium binding: a proposed mechanism for coupled calcium binding and protein polymerization. J Biol Chem. 2004; 279: 18026–18033. https://doi.org/10.1074/jbc.M311553200 PMID: 14871888

41. Fliegel L, Burns K, MacLennan DH, Reithmeier RA, Michalak M. Molecular cloning of the high affinity calcium-binding protein (calreticulin) of skeletal muscle sarcoplasmic reticulum. J Biol Chem. 1989; 264: 21522–21528. PMID: 2600080

42. Ostwald TJ, MacLennan DH. Isolation of a high affinity calcium-binding protein from sarcoplasmic retic-ulum. J Biol Chem. 1974; 249: 974–979. PMID: 4272851

43. Palmer AE, Jin C, Reed JC, Tsien RY. Bcl-2-mediated alterations in endoplasmic reticulum Ca2+ ana-lyzed with an improved genetically encoded fluorescent sensor. Proc Natl Acad Sci. 2004; 101: 17404–17409. https://doi.org/10.1073/pnas.0408030101 PMID: 15585581

44. Selvin D, Hesse E, Renaud J-M. Properties of single FDB fibers following a collagenase digestion for studying contractility, fatigue, and pCa-sarcomere shortening relationship. Am J Physiol—Regul Integr Comp Physiol. 2015; 308: R467–R479. https://doi.org/10.1152/ajpregu.00144.2014 PMID: 25568074

45. Michelucci A, Paolini C, Boncompagni S, Canato M, Reggiani C, Protasi F. Strenuous exercise triggers a life-threatening response in mice susceptible to malignant hyperthermia. FASEB J. 2017; fj.201601292R. https://doi.org/10.1096/fj.201601292R PMID: 28465322

46. Michalak M, Corbett EF, Mesaeli N, Nakamura K, Opas M. Calreticulin: one protein, one gene, many functions. Biochem J. 1999; 344 Pt 2: 281–292.

47. Rossi AE, Dirksen RT. Sarcoplasmic reticulum: the dynamic calcium governor of muscle. Muscle Nerve. 2006; 33: 715–731. https://doi.org/10.1002/mus.20512 PMID: 16477617

48. Yoshida M, Minamisawa S, Shimura M, Komazaki S, Kume H, Zhang M, et al. Impaired Ca2+ store functions in skeletal and cardiac muscle cells from sarcalumenin-deficient mice. J Biol Chem. 2005; 280: 3500–3506. https://doi.org/10.1074/jbc.M406618200 PMID: 15569689

49. Divet A, Paesante S, Grasso C, Cavagna D, Tiveron C, Paolini C, et al. Increased Ca2+ storage capacity of the skeletal muscle sarcoplasmic reticulum of transgenic mice over-expressing membrane bound calcium binding protein junctate. J Cell Physiol. 2007; 213: 464–474. https://doi.org/10.1002/jcp.21121 PMID: 17516551

50. Lamboley CRH, Kake Guena SA, Touré F, Hébert C, Yaddaden L, Nadeau S, et al. New method for determining total calcium content in tissue applied to skeletal muscle with and without calsequestrin. J Gen Physiol. 2015; 145: 127–153. https://doi.org/10.1085/jgp.201411250 PMID: 25624449

51. Y V et al. Accelerated activation of SOCE current in myotubes from two mouse models of anesthetic- and heat-induced sudden death.—PubMed—NCBI [Internet]. [cited 15 Nov 2017]. https://www.ncbi.nlm.nih.gov/pubmed/24143248

52. Boncompagni S, Michelucci A, Pietrangelo L, Dirksen RT, Protasi F. Exercise-dependent formation of new junctions that promote STIM1-Orai1 assembly in skeletal muscle. Sci Rep. 2017; 7: 14286. https://doi.org/10.1038/s41598-017-14134-0 PMID: 29079778

53. Launikonis BS, Ríos E. Store-operated Ca2+ entry during intracellular Ca2+ release in mammalian skeletal muscle. J Physiol. 2007; 583: 81–97. https://doi.org/10.1113/jphysiol.2007.135046 PMID: 17569733

54. Vecellio Reane D, Vallese F, Checchetto V, Acquasaliente L, Butera G, De Filippis V, et al. A MICU1 Splice Variant Confers High Sensitivity to the Mitochondrial Ca2+ Uptake Machinery of Skeletal Muscle. Mol Cell. 2016; 64: 760–773. https://doi.org/10.1016/j.molcel.2016.10.001 PMID: 27818145

55. Cortassa S, Aon MA, Marbán E, Winslow RL, O'Rourke B. An Integrated Model of Cardiac Mitochondrial Energy Metabolism and Calcium Dynamics. Biophys J. 2003; 84: 2734–2755. https://doi.org/10.1016/S0006-3495(03)75079-6 PMID: 12668482

56. Tran K, Smith NP, Loiselle DS, Crampin EJ. A Thermodynamic Model of the Cardiac Sarcoplasmic/Endoplasmic Ca2+ (SERCA) Pump. Biophys J. 2009; 96: 2029–2042. https://doi.org/10.1016/j.bpj.2008.11.045 PMID: 19254563